Surface-Mediated Selective Photocatalytic Aerobic Oxidation Reactions on TiO_2 Nanofibers

Lizhi Huang [a,b], Jianfeng Jia[c], Hongwei Liu[d], Zhanfeng Zheng[a,*] Yong Yuan[e], Jian Zhao[d], Yantao Zhang[a], Shuai Chen[a], Weibin Fan[a], Eric R. Waclawik[d], and Huaiyong Zhu[d]

[a] State Key Laboratory of Coal Conversion, Institute of Coal Chemistry, Chinese Academy of Sciences, Taiyuan 030001, Shanxi, China

[b] University of Chinese Academy of Sciences, Beijing 100049, China

[c] The School of Chemical and Material Science, Shanxi Normal University, Linfen 041004, Shanxi, China

[d] School of Chemistry, Physics and Mechanical Engineering Queensland University of Technology Brisbane, QLD 4000, Australia

[e] National Engineering Research Center of Clean Coal Combustion, Xi'an Thermal Power Research Institute Co. Ltd., Xi'an 710032, P.R. China

* Corresponding author. Tel./Fax.: +86 3154040605.

Email address: zf.zheng@sxicc.ac.cn (Z. Zheng)

Abstract

TiO_2 nanofibers were used in the selective photocatalytic aerobic oxidation of benzylamine and 4-methoxybenzyl alcohol. N-doped TiO_2 nanofiber shows lower aerobic oxidation activity than un-doped TiO_2 nanofibers, which was attributed to the reduction of O_2 adsorption energy around the nitrogen site as indicated by the density functional theory (DFT) calculations when three-coordinated oxygen atoms are substituted by nitrogen atoms. It is found that the activity can be recovered by a controlled calcination of the N-doped NFs in air. The dependence of the conversion of benzylamine and 4-methoxybenzyl alcohol on the intensity of light irradiation confirms that these two reactions are driven by light. Action spectra show that the two oxidation reactions are responsive to light up to the visible light irradiation range, which is due to the formation of surface complex by the adsorption of reactants onto the surface of the catalysts evidenced by the in-situ IR experiments. Moreover, temperature shows positive influence on the oxidation activity. Both catalytic and in-situ IR results reveal that benzaldehyde is the intermediate in the aerobic oxidation of benzylamine to N-benzylidenebenzylamine process.

Keywords

N-doped TiO_2; surface complex; photocatalysis; DFT; aerobic oxidation

1. Introduction

Titanium dioxide (TiO_2) is one of the most promising photocatalysts for the removal of organic contaminants from waste water and polluted air due to its high efficiency, stability and non-toxicity[1-5]. In order to use TiO_2 practically in environmental treatment and organic synthesis, there are still some difficulties to overcome. Firstly, the active phase of TiO_2, anatase, absorbs light only in the UV range of the electromagnetic spectrum (TiO_2 band gap 3.2 eV, ~4% of the total solar energy)[6-8]. In contrast to the UV, the visible region of the solar spectrum accounts for nearly 43% of solar energy incident on the earth's surface. To utilise solar energy efficiently, methods such as doping non-metal elements N, C, S, P, F, B into the lattice of TiO_2 to shift the light absorption to the visible have been extensively studied in recent years[9-15]. Most of such researches focused on the doping-induced band structure change[16-24] and its consequence on light absorption, while few studies have been conducted on the changes in detail surface properties such as composition and structures and the impact of the changes on the catalytic performance. The performance of a photocatalyst does not entirely depend on the light absorption. As we found in the present study, although N-doped TiO_2 exhibit better visible light absorption than the undoped counterpart, the performance of the doped sample is poorer even under visible light. Since the reaction takes place on catalyst surface, the surface properties can significantly affect the catalytic activity. For example, the ability of the surface to adsorb O_2, the oxidant for many oxidation reactions, may determine the performance of catalysts for the oxidation[25]. On the other hand, doping with other elements certainly results in the changes in the surface property, which should influence the catalytic performance. It is also known some organics strongly adsorb on the TiO_2 surface (forming a surface complex), and act as a sensitizer that allows the system to absorb visible light. The formation of the surface complexes capable of

absorbing visible light have been utilised to develop photocatalysts for selective oxidation of toluene under room temperature[26]. Furthermore, TiO_2 generally exhibits poor selectivity in photocatalytic oxidation reactions due to its high oxidation power in aqueous[27-29]. This is a merit when TiO_2 is used for an environmental remediation purpose as all organic contaminants can be decomposed to CO_2 and H_2O. But when it is used in photocatalytic synthesis, the poor selectivity is a serious disadvantage. Recently, significant efforts have been made to improve selectivity of TiO_2 photocatalysts in organic solvents for synthesis of fine organic chemicals[30-32]. For this purpose, the interaction of surface OH groups with photo-generated holes should be hindered. For organic synthesis, the selectivity to desired product is a criterion of equal importance to the conversion rate of the reactant, determining the efficiency of the synthesis. Therefore, to achieve green processes of photocatalytic organic synthesis, such as selective aerobic oxidation of organic compounds, it is important to understand the impact of the surface property of photocatalysts on their performance, and thus we can tune the surface structure to optimise photocatalysts for organic synthesis driven by light irradiation.

In the present study, we report the synthesis of anatase nanoplates covered TiO_2(B) core-shell nanofibers by the calcination of protonated-titanate (H-titanate) in air or gaseous NH_3 flow (designated as BF and N-BF, respectively) at elevated temperatures. The calcination in NH_3 introduces N to the anatase shell surface, and reduces the surface OH groups. The N-BF NFs was calcined in air for varying periods (20 and 180 min, designated as N-BF-A20 and N-BF-A180) to tune the amount of the surface N sites. The oxygen adsorption ability on the surface of N-doped and undoped TiO_2 NFs was studied by density functional theory (DFT). Two aerobic oxidation reactions, the aerobic oxidation of benzylamine and 4-methoxybenzyl alcohol, were chosen to examine the influence of the surface on the photocatalytic activity.

2. Experimental

2.1. Nitrogen doping and surface post-treatment

The H-titanate ($H_2Ti_3O_7$) nanofibers were prepared by the hydrothermal reaction between anatase powders and concentrated NaOH solution, followed by an acid wash process. TiO_2(B) nanofibers were prepared by direct calcination of the H-titanate nanofibers at 550 °C in air (denoted as BF). To prepare the N-doped TiO_2, a quartz boat, loaded with H-titanate nanofibers, was placed in a quartz tube (30 mm in diameter) at a constant temperature zone of a tube furnace. The system was heated to a 550 °C in gaseous NH_3 flow (50 standard cubic centimeters per minute (SCCM), controlled with a flow meter). After reaction, the furnace was cooled to room temperature naturally with continuous NH_3 gas flow (denoted ad N-BF). The N-doped sample was then calcined in air at 550 °C for different periods from 20 min and 3 h to remove adsorbed NH_3 and obtain partial oxidization of the N-doped surface and labeled N-BF-A20, and N-BF-A180.

2.2. Characterization

The transmission electron microscopy (TEM) studies on the samples were carried out on a FEI Tecnai F20 operating at 200 kV. X-ray diffraction (XRD) patterns of the samples were recorded on a Philips PANalytical X'Pert PRO diffractometer using Cu Kα radiation (λ = 1.5418 Å) operating at 40 kV and 40 mA with a fixed slit. Infrared spectra of the samples were obtained using a Nicolet Nexus 870 FTIR spectrometer with a smart endurance single bounce diamond ATR cell. Spectra over the 4000 to 525 cm^{-1} range were obtained by the co-addition of 64 scans with a resolution of 4 cm^{-1}. Nitrogen adsorption isotherms were measured by the volumetric method on an automatic adsorption instrument (Micromeritics, Tristar 3000) at liquid nitrogen temperature (77 K). Specific surface area was calculated by the Brunauer-Emmett-Teller (BET)

method from the data in a P/P_0 range between 0.05 and 0.2. To investigate the light absorption and emission behavior of the samples, the diffuse reflectance UV-Visible (Dir-UV-Vis) spectra of the samples were measured on a Varian Cary 5000 spectrometer. In-situ FT-IR spectra of the samples before and after light irradiation were recorded on a Bruker Tensor 27 IR spectrometer equipped with a MCT detector. Prior to the measurement, the sample was palletized into self-supporting wafer, introduced into an in-situ IR cell equipped with CaF_2 windows, and pretreated at 10^{-2} Pa and 400 ^{o}C for 2 h. Subsequently, the sample was exposed to benzylamine or 4-methoxybenzyl alcohol vapor (25 Pa) at room temperature. The residual reactants were removed under evacuation and dry air (50 KPa) was introduced into the in-situ IR cell. The time course IR spectra were recorded after Xe light irradiation.

2.3. Selective photocatalytic oxidation

The light source was a 100 W COB LED lamp (white light, the spectrum is shown in Fig. S1) or a 300 W Xe lamp (CEL-HXF 300, Beijing CEL Tech. Co., Ltd, the spectrum is shown in Fig. S2). The long pass filters and optical band pass filters were used to block light of other wavelengths to study the wavelength irradiation contribution. All the oxidation reactions were conducted under oxygen atmosphere (1 atm) and O_2 was bubbled through the vessel for 1 min prior to the catalytic reaction. After reaction, the liquid products were analyzed using a Shimadzu 2014C GC with a WondaCap 5 column.

Photocatalytic oxidation of benzylamine: Typically, benzylamine (0.2 mmol) was dissolved in CH_3CN (5 ml) and the photocatalyst (50 mg) was added. Then the reaction mixture was kept at 40 °C and illuminated with LED light for 5 h.

Photocatalytic oxidation of 4-methoxybenzyl alcohol: In a typical reaction, catalyst (50 mg) was added into 5 ml mixed solution of (50 ml CH_3CN and 2 mmol 4-methoxybenzyl alcohol). The system was kept at 40 °C and illuminated under Xe light for 4 h.

2.4. Theoretical calculation

The relationship between the TiO_2 surface structure and its ability to adsorb O_2 was explored using density functional theory (DFT) calculations which were performed by CP2K package [http://www.cp2k.org/](See supporting information Table S1 for detailed calculation parameters). In the DFT calculations, the electron exchange-correlation was described by the revised GGA-PBE functional[33], and DFT-D3 van der Waals correction[34] was considered. Spin polarization was included whenever necessary. Based on the experimental data, the 100 surface of anatase TiO_2 was simulated. The calculations were carried out on periodic slabs in a (5×2×4) supercell that comprised 160 TiO_2 units and separated by a vacuum of more than 1.30nm (see Fig. S3 for the cell structure in the supporting information). To mimic bulk constraints, the bottom layer of the TiO_2 slab was fixed and the *a* and *b* lattice parameters were fixed to the experimental lattice constants.

3. Results and discussion

3.1. Surface and structure properties of TiO_2 and N-doped TiO_2 nanofibers (NFs)

All TiO_2 nanofiber samples (BF, N-BF, N-BF-A20 and N-BF-A180) inherited the fibril morphology from the titanate NFs according to TEM observation and the BET surface area for these fibers were almost the same at ca. 30 m^2g^{-1} due to their same calcination temperature of 550 °C. Fig. S4 shows the XRD patterns of these nanofibers. The main diffraction peaks were indexed to the TiO_2(B) phase (monoclinic, space group *C*2/*m*, identical to ICDD PDF No. 74-1940) (Fig. S4). It is noted that the calcination at 550 °C caused phase conversion from the

TiO_2(B) to anatase phase (tetragonal, space group $I4_1/amd$, ICDD PDF No. 21-1272) in a small fraction (ca. 3%, calculated according to the equation in reference 31) of the fibers[35]. This conversion took place only at the surface of the N-doped nanofibers, yielding anatase nanoplates covering the fibers (Fig. 1A). The electron diffraction pattern of BF still shows a typical TiO_2(B) feature (Fig. 1B). It can be deduced, through the FFT and IFFT treatment of the HRTEM image of BF NFs (Figs. 1C-E), that the direction $[\bar{1}10]_B$ is parallel to $[111]_A$, where "A" and "B" represent anatase and TiO_2(B), respectively. There is a good planar match between anatase nanoplates and TiO_2(B) nanofiber, with $(011)_A$ parallel to $(200)_B$. Therefore, the exposed surfaces of the nanofibers are mainly anatase (100) facets. The anatase nanoplates are bonded solidly to the fiber substrate by chemical bonds (sharing the oxygen atoms at the interface between the two phases).

{Fig. 1}

As can been seen clearly from the UV-Vis spectra (Fig. S5A), after nitrogen doping, the light absorption extends to the visible range for N-BF NFs. This is caused by partial substitution of O atoms for N atoms on the surface and in the bulk of TiO_2 structure resulting in reduction of the band gap of the material and a red shift of light absorption by the solid[9, 18]. Except for the surface N content, both $-NH_x$ groups and -OH groups exist on the surface of the N-doped sample, confirmed by IR spectra (Fig. S5B). The calcination of N-BF in air caused the loss of N content from the bulk and surface structure, leading to decreased absorption in the UV-Vis spectra (Fig. S5A).

3.2. Photocatalytic performance on different surfaces

To investigate the influence of the surface property on the reaction activity, two oxidation reactions, the aerobic oxidation of benzylamine and 4-methoxybenzyl alcohol, were chosen and

the activity of TiO_2 fibers with different surfaces were examined under light irradiation. In this study, no conversion was observed in the absence of TiO_2 nanofibers under light irradiation which confirms that the reactions are catalyzed by TiO_2 nanofibers.

{Fig. 2}

The photocatalytic performances of TiO_2 (BF) and N-doped TiO_2 (N-BF, N-BF-A20, and N-BF-A180) NFs for the aerobic oxidation of benzylamine and 4-methoxybenzyl alcohol are illustrated in Fig. 2. The N-BF NFs exhibited much lower activity (conversion at 60%) for the selective oxidation of benzylamine to *N*-benzylbenzaldimine, compared to the nanofibers calcined in air (91% conversion for BF). After N-BF was calcined in air for 20 and 180 min, the conversion rate gradually increased to 89% and 97%. A similar situation is also observed for the selective oxidation of 4-methoxybenzyl alcohol to the corresponding aldehyde under Xe light illumination using these nanofibers: the conversions on BF, N-BF, N-BF-A20 and N-BF-A180 are 96%, 60%, 96% and 99% respectively. Following the calcination in air at 550 °C (N-BF-A20 and N-BF-A180), the doped N sites on the external surface of the nanofibers were replaced by O and thus the O_2 adsorption and catalytic activity was regenerated. It is deduced that the oxidized surface is advanced for the aerobic oxidation reactions and therefore BF and N-BF NFs with different surfaces were compared in the following study.

The dependence of the conversion of benzylamine and 4-methoxybenzyl alcohol on the intensity of light irradiation catalysed by BF and N-BF NFs shows that the conversion increases almost linearly as the irradiance is raised (Fig. 3A and Fig. 4A). Comparative experiments in the dark reactions are also carried out and no conversions are observed. It is clearly demonstrated that the oxidation of benzylamine/4-methoxybenzyl alcohol is driven by light.

{Fig. 3}

As shown in Fig. S5A, the N doped nanofibers exhibit much stronger light absorption than the undoped counterpart in the visible range due to the hybridization states at the top of the valence band originating from nitrogen 2*p* states and oxygen 2*p* states or the mid-gap level created by the introduction of N[9, 13, 36]. However, this absorption does not appear to be the sole factor determining the photocatalytic activity under visible light. It can be seen from Fig. 5B that the oxidation activity of benzylamine on BF is superior to that on N-BF in the visible light irradiation range which cannot be explained by the ability of light absorption. Consequently, this implies that the activity under visible light may not only depend on the band structure of TiO_2 in the present study. It is interesting to find that the adsorption of benzylamine or 4-methoxybenzyl alcohol on BF or N-BF NFs causes the absorption extension to the visible range in the UV-vis spectra (Fig. S6). Pure benzylamine can only absorb light bellow 300 nm and bare anatase TiO_2 can only absorb light bellow 385 nm in the previous literature[37]. Hence, the enhanced light absorption is reasonably attributed to the complex formed by the interaction of benzylamine with the TiO_2 surface[32, 37-40]. The surface complex excites an electron from the N localized on the amide nitrogen to the conduction band of TiO_2 under light illumination with a much longer wavelength, which is so called the ligand-to-metal charge transfer (LMCT) mechanism. The activities in the visible range are possibly related to the surface complexes formed on the BF and N-BF surfaces[41]. Then the action spectra of these two reactions on BF and N-BF NFs are studied (Fig. 3B and Fig. 4B). The light source was Xe lamp with optical band pass filters and the irradiance intensity was maintained at 0.035 Wcm^{-2}. The results clearly show that the activity gradually decreased with the increasing irradiation wavelength. The conversion of the reactants as a function of the wavelength of the incident light (action spectra) does not match with the UV-vis spectra of bare BF and N-BF NFs (Fig. S6). And the two reactions are responsive to light up

to 520 nm, which is much smaller than the band gap absorption of TiO_2 (band gap at 3.2 eV, corresponding to absorption at 387.5 nm). The differential spectra between before and after reactants adsorption were also given in the action spectra (Fig. 3B and Fig. 4B). It is found that a new absorption band appeared at about 350 nm with long tail up to 450 nm. These new bands could be reasonably ascribed to the surface complexes. When the reaction temperature was increased from 40℃ to 60℃ (Fig. S7), the aerobic oxidation activities were enhanced greatly in the UV region (wavelength shorter than 400 nm) but only a little in the visible range. In Fig. 4B, N-BF NFs shows a better catalytic activity to BF NFs in the oxidation of 4-methoxybenzyl alcohol in the visible light irradiation range while BF NFs shows higher activity than N-BF NFs both in the UV and visible light irradiation range in the oxidation of benzylamine as shown in Fig. 3B. In the present study, the O_2 adsorption capability and the light absorption capability would affect the reaction activity when the reaction temperature, the light intensity and wavelength were fixed. As suggested by the DFT results (Section 3.3) and UV-vis spectra (Fig. S5A), BF exhibits higher O_2 adsorption capability but weaker visible light absorption. The same trend was observed in the UV and visible range when BF and N-BF were applied to the selective oxidation of benzylamine. It is deduced that O_2 adsorption capability plays the dominant role in this oxidation. On the other hand, the strong light absorption of N-BF in the visible range is supposed to be the crucial factor that affects the 4-methoxybenzyl alcohol oxidation reaction in the visible range.

The reaction kinetic data obtained at various temperatures (25, 40 and 60 °C) for the oxidation of benzylamine and 4-methoxybenzyl alcohol using BF and N-BF NFs under UV and visible light irradiation are summarized in Figs. 3C-D and Figs. 4C-D. Both reactions exhibit a typical zero-order kinetic reaction. The reaction rate increased gradually when the reaction

temperature was increased from 25 to 60 °C. Generally, a semiconductor photocatalyst exhibits negative temperature effect due to the increase of the recombination rate[42]. The result further confirms that the complex works in a different mechanism. The reaction rate constants of the oxidation of benzylamine on BF at 25, 40 and 60 °C under UV light irradiation (from 320 to 415 nm) are 2.17 $\times 10^{-6}$ mol·L^{-1}·s^{-1}, 3.14 $\times 10^{-6}$ mol·L^{-1}·s^{-1} and 3.64 $\times 10^{-6}$ mol·L^{-1}·s^{-1}, calculated from the slope by plotting the conversion against the reaction time. While visible light irradiation (> 420 nm) can also drive the aerobic oxidation of benzylamine but in a much lower rate (3.33 $\times 10^{-7}$ mol·L^{-1}·s^{-1} at 25 °C, 5.28 $\times 10^{-7}$ mol·L^{-1}·s^{-1} at 40 °C and 8.89 $\times 10^{-7}$ mol·L^{-1}·s^{-1} at 60 °C, respectively). Benzylamine was converted to *N*-benzylbenzaldimine with a very high selectivity (> 95%) regardless of the reaction temperature. Benzaldehyde was also detected in the product during the reaction which may indicate that benzaldehyde is the intermediate product and converts to imine through condensation reaction with another benzylamine molecule[40]. The conversions of 4-methoxybenzyl alcohol over BF were also carried out (Fig. 5B). The same tendency of this reaction was observed as that of oxidation of benzylamine. The higher the reaction temperature, the faster the oxidation reaction proceeded. The estimated apparent activation energy (E_a) for the oxidation of benzylamine and 4-methoxybenzyl alcohol under UV-light irradiation and visible light irradiation was displayed in Table S2. It is observed that these two aerobic oxidation reactions on N-BF show no apparent dependence on the photo-energy (17 kJ mol^{-1} vs. 15 kJ mol^{-1} for oxidation of benzylamine, 14 kJ mol^{-1} vs. 14 kJ mol^{-1} for oxidation of 4-methoxybenzyl alcohol in the UV range and visible range on N-BF). Photo-energy has an obvious influence on E_a for the aerobic oxidation reactions on BF. The estimated apparent activation energy is 12 kJ mol^{-1} for benzylamine under UV-light irradiation, while it is 23 kJ mol^{-1} under visible light irradiation. It was reported that the apparent activation energy for the

selective oxidation of benzylamine to *N*-benzylbenzaldimine on Au-Pd@ZrO_2 catalyst in the dark and under visible light irradiation was 131.5 and 118.4 kJ mol^{-1}, respectively[43]. Therefore, the photocatalytic reaction for the oxidation of benzamine on TiO_2 nanofibers has smaller activation energy and can proceed readily.

From the above analysis, the activity is apparent not from charge separation in the TiO_2 and subsequent interaction with the reactants. This indicates that the TiO_2 nanofibers play an important role in the catalytic process and so it is deemed to investigate the interaction between the reactant molecules with the nanofibers. Both of the benzylamine oxidation reaction and 4-methoxybenzyl alcohol oxidation involve the adsorption of the molecule and O_2. Recently we have found that the anatase surface has a strong ability to generate surface hydroxyl groups[25]. Liu et al.[44] found that the OH groups at the (110) surface of anatase TiO_2 can facilitate O_2 adsorption on TiO_2, and such absorbed O_2 may diffuse to the active site for reactions. Therefore, O_2 adsorption properties on N-doped and undoped TiO_2 surfaces were correlated to the surface –OH groups and were explored using density functional theory (DFT) calculations.

{Fig. 4}

3.3. Investigation of surface O_2 adsorption by density functional theory (DFT) calculation

The perfect (100) surface of TiO_2 was considered first in this work. The results showed that O_2 is hardly adsorbed on the (100) surface with an optimized adsorption energy of only 0.03 eV. With one OH bound on the surface as shown in Figure 1a, the adsorption energy increases slightly to 0.16 eV. Both experimental and theoretical investigations[45-49] showed that a H_2O molecule can be adsorbed by an oxygen vacancy on the TiO_2 surface, and then dissociate to two adjacent OH groups. Based on this knowledge, the adsorption of O_2 on the TiO_2 surface with two adjacent OH groups were considered as shown in Fig. 5b and Fig. 5c. In Fig. 5b, the O_2 molecule

was adsorbed on Ti atoms nearby the OH groups. The calculated adsorption energy was 0.90 eV and the bond length of O_2 increased to 1.42 Å, significantly longer than the free O_2 molecule (1.23 Å) and the O_2 (1.33 Å) in Fig. 5a. The O-Ti distance is in a range of 1.90 to 1.93 Å, which is shorter than that in Fig. 5a. Both the O_2 bond length and O-Ti distance indicate that the O_2 in Fig. 5b is adsorbed more strongly by the TiO_2 surface than that in Fig. 5a. These results show that pairs of OH groups can facilitate O_2 adsorption on the TiO_2 (100) surface. This is analogue to the study by Liu et al.[44] that the OH groups at the (110) surface of anatase TiO_2 can facilitate O_2 adsorption on TiO_2. Another interesting question to be answered is whether the OH effect on O_2 adsorption is long-ranged. For demonstration purposes, only one situation was considered in our work as shown in Fig. 5c, in which O_2 is located more remote from the OH group than that in Fig. 5b. The calculated adsorption energy was 0.78 eV, only slightly lower than that of Fig. 5b. Liu et al. had also performed a detailed investigation showing that OH group on TiO_2(110) possesses a long-range effect on O_2 adsorption.

{Fig. 5}

In our experiments, both O-H and N-H vibrations were observed in IR spectrum (Fig. S5). We hypothesise that when a NH_3 molecule is captured by an oxygen vacancy on the TiO_2 surface, as occurred for H_2O, it will dissociate to one NH_2 group and an adjacent OH group. Three O_2 adsorption styles were considered on as formed N-doped TiO_2(100) surfaces, as shown in Figs. 5d-f. In Fig. 5d, O_2 is adsorbed on two Ti atoms in a bridge style with adsorption energy of 0.84eV. The O_2 bond length is 1.41 Å and Ti-O distance is about 1.91~1.92 Å, which are both similar to the situation in Fig. 5e and Fig. 5f. This result indicates that replacement of one OH by NH_2 does not significantly impact the O_2 adsorption on TiO_2(100) surface. In Figs. 5e and 5f, O_2 is adsorbed on the top of different Ti atoms. The calculated adsorption energies are 0.91 and

1.11eV, respectively. The adsorption energies in all these three situations are on the same order as that on the TiO_2 surface with a pair of OH groups as shown in Fig. 5b and Fig. 5c. Hence, the lower activity of the N-doped TiO_2, observed in our experiment is unlikely to be caused by this type of surface structures of the doped nitrogen atom as we reported in the previous study[36].

It is reasonable to assume that when the titanate is reacted with NH_3 to give a N-doped TiO_2 nano-structure, the nitrogen atoms may replace some three-coordinated oxygen atoms on the TiO_2 surface as shown in Figs. 5g-h. In Fig. 5g, a nitrogen atom replaces an oxygen atom nearby the OH groups, and in Fig. 5h, it replaces an oxygen atom a short distance from the OH groups. Interesting calculation result was obtained for the both surface structures: the O_2 adsorption energies were markedly decreased. The calculated adsorption energies associated with Fig. 5g and Fig. 5h were 0.15 and 0.05eV, respectively. In Fig. 5g the Ti-O distances were 2.17 Å and 2.23 Å, while the O_2 bond length was 1.33 Å. In Fig. 5h, the shortest Ti-O distance was 3.83 Å and the O_2 bond length was 1.23 Å. These calculations show that when three-coordinated oxygen atoms are substituted by nitrogen atoms, the O_2 adsorption energy around the nitrogen site will be reduced considerably. The work of Liu et al. indicated that O_2 adsorption and supply play an important role in the reaction on the TiO_2 surface. The small adsorption energy indicates that O_2 will desorb readily from the surface in the vicinity of such doped nitrogen sites. The lower activity of the N-doped TiO_2 surface in the oxidation reaction involving O_2 is highly likely due to the weak O_2 adsorption ability of such doped-in nitrogen atoms.

3.4. FT-IR observation of surface adsorbed species and the change during photoirradiation

For the benzylamine oxidation reaction, the surface adsorption of the reactant was studied by in-situ FT-IR spectroscopy (Fig. 6). After exposing to benzylamine vapor at 25 Pa, the intensity of band at 1585 cm^{-1} increased with time on both BF and N-BF (Figs. 6A and 6C). And this band

was attributed to the NH_2 bending vibration (δ_{sNH2})[50]. Furthermore, the bands at 1142 and 1069 cm^{-1} for BF and 1157 and 1065 cm^{-1} for N-BF assigned to C-N stretching vibration (ν_{C-N}) increased with time. The same tendency was observed for the bands at 1381 and 1454 cm^{-1} for BF and 1374 and 1454 cm^{-1} for N-BF corresponding to CH_2 bending vibrations, and the ones at 1499 and 1543 cm^{-1} for both BF and N-BF attributed to C-C stretching vibrations of an aromatic ring. The observations obtained from the in-situ IR spectra revealed that benzylamine adsorbed on the surface of BF and N-BF in the form of molecules.

After benzylamine was adsorbed in-situ on BF and N-BF, dry air was introduced into the in-situ IR cell and followed by irradiation with Xe lamp for various times. The changes in FT-IR spectra during the irradiation process were recorded as shown in Fig. 6B and 6D. The spectra given in Fig. 6B and 6D are difference spectra, where positive peaks indicate newly-formed products and negative peaks indicate consumed reactants. The black arrows shows the bands related to ν_{C-N} (1061 cm^{-1}), ω_{CH2} (1350 cm^{-1}), δ_{sCH2} (1457 cm^{-1}), ν_{C-C} (1499 cm^{-1}), and δ_{sNH2} (1615 and 1578 cm^{-1}), which belong to benzylamine, decreased in intensity with increasing irradiation time. In order to confirm the newly-formed bands, benzaldehyde was adsorbed on BF and N-BF in-situ (Fig. 6B(a) and Fig. 6D(a)). The bands at 1651, 1530 and 1414 cm^{-1} are attributed to $\nu_{C=O,}$ ν_{C-C}(aromatic), and δ_{sCHO}, which clearly show that benzaldehyde was formed during the benzylamine conversion (Fig. 6B and Fig. 6D). After irradiation, the system was evacuated for another 30 min and the FT-IR spectra do not change much, which means benzaldehyde were still adsorbed on catalysts after the evacuation.

The similar in-situ IR experimental procedure was carried out for the reaction of 4-methoxybenzyl alcohol. After exposing to 4-methoxybenzyl alcohol at 25 Pa, the bands growing in at 1612, 1512, 1456, 1302, 1252, 1229, 1177 (or 1179) and 1042 cm^{-1} on BF and N-BF (Figs.

7A and 7D) are similar to the previous literature[51]. The bands at 1612, 1512 and 1456 cm^{-1} are ascribed to skeletal vibrations of the aromatic and the band at 1229 cm^{-1} can be assigned to the C-C stretching vibration[52]. The two bands centered at 1252 and 1042 cm^{-1} correspond to the asymmetric and symmetric C-O-C stretching vibration of the methoxy group attached to benzene ring[50]. Another band appears at 1137 cm^{-1} for BF and 1164 cm^{-1} for N-BF, which was not observed in the previous ATR-FTIR study of the adsorption of 4-methoxybenzyl alcohol[51]. It is likely to assign this band to the alcoholate species formed by the interaction between the surface Ti and the adsorbed 4-methoxybenzyl alcohol[26, 52]. Thus, according to the observed changes of IR bands, it is suggested that 4-methoxybenzyl alcohol adsorbed on the surface of BF and N-BF and the -CH_2-OH group would interact with Ti to form alcoholate species –CH_2-O(H)-Ti.

After introducing dry air, the sample after 4-methoxybenzyl alcohol adsorption was illuminated with Xe light (Figs. 7C and 7F). As irradiation continues, the bands related to reactant 4-methoxybenzyl alcohol, such as 1612, 1512, 1456 (skeletal vibrations of the aromatic) and 1252 cm^{-1} (asymmetric C-O-C stretching vibration) decreased in intensity. In the meantime, some newly-formed bands were also observed during the irradiation as marked by the red arrows in Fig. 7. The positions of the newly-formed bands are in good agreement with those of the 4-methoxybenzaldehyde adsorbed on BF and N-BF. Specifically, the typical bands of 4-methoxybenzaldehyde related to the $\nu_{C=O}$ (1655 cm^{-1}), ν_{C-C}(aromatic)(1603, 1576 and 1512 cm^{-1}), and δ_{sCHO} (1400 cm^{-1}) are observed.

{Fig. 6} & {Fig. 7}

3.5. Proposed mechanism

BF and N-BF exhibit a better activity for the oxidation of benzylamine and 4-methoxybenzyl alcohol under UV irradiation which is in consistence with the light absorption ability. The N-BF NFs exhibits a stronger absorption in the visible range compared to BF, but N-BF exhibits a weak activity compared to BF for the oxidation of benzylamine. This indicates that the activity in the visible range is not directly related to the light absorption. In addition, the O_2 adsorption ability is different: BF has a stronger ability for the adsorption of O_2. In order to further clarify the importance of O_2 in the selective oxidation of benzylamine and 4-methoxybenzyl alcohol, similar oxidation experiments were carried out in the absence of O_2. Only negligible conversions of benzylamine and 4-methoxybenzyl alcohol (less than 3% reactants conversions) at 25 °C for BF and N-BF were observed in the absence of O_2. And the poor catalytic activities show no improvements even raising the temperature to 60 °C. However, when reactor was re-exposure to O_2 after eliminating gas in the reaction system, the reaction activity recovered. Additionally, the color of the catalyst which changed to dusty blue infers the formation of Ti^{3+} center[53]. This indicates without O_2 involving in the reaction system, Ti^{4+} acted as the electron acceptor instead of O_2 and itself was reduced to Ti^{3+}. The intact catalytic cycle could not be completed without the further oxidation of Ti^{3+} to Ti^{4+}. Thus, taking these results into consideration, O_2 is indispensable in the photo-oxidation of benzylamine and 4-methoxybenzyl alcohol. Therefore, O_2 adsorption and activation on the surface is the key step of oxidation reactions.

Based on the above analysis and previous reported results, we tentatively propose a mechanism depicted in Fig. 8. For the aerobic oxidation of benzylamine, firstly, the reactant benzylamine is adsorbed on the surface of TiO_2 nanofibers to form surface charge transfer complex. Secondly, hole and electron would be generated on the surface charge transfer complex under light illumination. The photo-generated hole induces the H^+ subtraction form N of

benzylamine and photo-generated electron transfers to the conduction band of TiO_2, resulting in the formation of an amide radical and the reduction of Ti^{4+} to Ti^{3+}. The nitrogen-centered radical would rearrange via intramolecular H-abstraction to form a more stable carbon-centered radical[54, 55]. The following steps are analogous as previous investigations reported by Zhao, et. al[31, 32, 40, 56]. Thirdly, O_2 adsorbed on the surface of catalysts forms an intermediate possessed five-member-ring structure with carbon radical and Ti^{3+}. Fourthly, the cleavage of the C-N bond of benzylamine and the O-O bond of oxygen occurs to form benzaldehyde and a Ti-bonded three-member-ring structure. The produced benzaldehyde then further follows a condensation reaction with unreacted benzylamine to yield imine. Finally, the photocatalytic cycle are completed by the regeneration of Ti^{4+} sites on the surface of BF and N-BF NFs through the desorption of NH_2-OH molecule. The selective photocatalytic aerobic oxidation of 4-methoxybenzyl alcohol on BF and N-BF NFs is supposed to follow the similar pathway (Fig. 8B).

{**Scheme 1**}

4. Conclusion

It is found that nitrogen doping in TiO_2 NFs affects the photocatalytic oxidation process. The N-doped TiO_2 exhibits a lower activity for the oxidation of benzylamine and 4-methoxybenzyl alcohol compared to undoped TiO_2. The N-doped TiO_2 surface was demonstrated to have a poor ability to adsorb O_2 molecules according to the DFT calculation. The undoped TiO_2 or a controlled calcination of the N-doped NFs in air was necessary to restore the anatase surface for activation of oxygen molecules. The influences of intensity, wavelength and temperature on the activity of the aerobic oxidation reactions were investigated. The activities show linear increases as the irradiance is increased while gradually decreased as the wavelength prolonged. The

temperature effect was studied in the UV and visible range, respectively. The oxidations of benzylamine and 4-methoxybenzyl alcohol proceeding on N-BF show no apparent dependence on the photo-energy. The charge transfer surface complex was carefully examined by the measurement of UV-vis and in-situ FTIR spectroscopies. The activities in the visible light irradiation range were confirmed to be driven by the light absorption of the charge transfer surface complex. The results of this study not only demonstrate the great impact of surface properties of the TiO_2 NFs on their photocatalytic performance, but also reveal that tuning the surface structure of photocatalysts could be an effective method to optimise the photocatalytic activities of green processes for synthesis of fine organic chemicals.

Acknowledgements

Financial support from the Institute of Coal Chemistry (ICC), (Grant No. Y3SC821651 and J14-15-605) and Australian Research Council (ARC) are gratefully acknowledged.

References

[1] M. Anpo, P.V. Kamat, Environmentally Benign Photocatalysts: Applications of Titanium Oxide-based Materials, Springer, London, 2010.

[2] M.A. Fox, M.T. Dulay, Chem. Rev. 93 (1993) 341-357.

[3] M.R. Hoffmann, S.T. Martin, W.Y. Choi, D.W. Bahnemann, Chem. Rev. 95 (1995) 69-96.

[4] A.L. Linsebigler, G.Q. Lu, J.T. Yates, Chem. Rev. 95 (1995) 735-758.

[5] T.L. Thompson, J.T. Yates, Chem. Rev. 106 (2006) 4428-4453.

[6] T. Kawahara, Y. Konishi, H. Tada, N. Tohge, J. Nishii, S. Ito, Angew. Chem. Int. Ed. 41 (2002) 2811-2813.

[7] M. Zukalova, M. Kalbac, L. Kavan, I. Exnar, M. Graetzel, Chem. Mater. 17 (2005) 1248-1255.

[8] M. Gratzel, Nature 414 (2001) 338-344.

[9] R. Asahi, T. Morikawa, T. Ohwaki, K. Aoki, Y. Taga, Science 293 (2001) 269-271.

[10] S.C. Moon, H. Mametsuka, S. Tabata, E. Suzuki, Catal. Today 58 (2000) 125-132.

[11] S. Sakthivel, M. Janczarek, H. Kisch, J. Phys. Chem. B 108 (2004) 19384-19387.

[12] T. Umebayashi, T. Yamaki, H. Itoh, K. Asai, Appl. Phys. Lett. 81 (2002) 454-456.

[13] T. Umebayashi, T. Yamaki, S. Yamamoto, A. Miyashita, S. Tanaka, T. Sumita, K. Asai, J. Appl. Phys. 93 (2003) 5156-5160.

[14] Y. Zhou, P.W. Liu, W.Y. Zhang, M.Y. Xing, J.L. Zhang, Appl. Catal. B-Enviorn. 170-171 (2015) 66-73.

[15] V. Trevisan, A. Olivo, F. Pinna, M. Signoretto, F. Vindigni, G. Cerrato, C.L. Bianchi, Appl. Catal. B-Enviorn. 160–161 (2014) 152-160.

[16] R. Bacsa, J. Kiwi, T. Ohno, P. Albers, V. Nadtochenko, J. Phys. Chem. B 109 (2005) 5994-6003.

[17] O. Diwald, T.L. Thompson, T. Zubkov, E.G. Goralski, S.D. Walck, J.T. Yates, J. Phys. Chem. B 108 (2004) 6004-6008.

[18] H. Irie, Y. Watanabe, K. Hashimoto, J. Phys. Chem. B 107 (2003) 5483-5486.

[19] D. Li, H. Haneda, S. Hishita, N. Ohashi, Chem. Mater. 17 (2005) 2588-2595.

[20] R. Nakamura, T. Tanaka, Y. Nakato, J. Phys. Chem. B 108 (2004) 10617-10620.

[21] T. Sano, N. Negishi, K. Koike, K. Takeuchi, S. Matsuzawa, J. Mater. Chem. 14 (2004) 380-384.

[22] H. Tokudome, M. Miyauchi, Chem. Lett. 33 (2004) 1108-1109.

[23] J. Wang, D.N. Tafen, J.P. Lewis, Z. Hong, A. Manivannan, M. Zhi, M. Li, N. Wu, J. Am. Chem. Soc. 131 (2009) 12290-12297.

[24] M.C. Yang, T.S. Yang, M.S. Wong, Thin Solid Films 469-70 (2004) 1-5.

[25] Z.F. Zheng, J. Teo, X. Chen, H.W. Liu, Y. Yuan, E.R. Waclawik, Z.Y. Zhong, H.Y. Zhu, Chem.-Eur. J. 16 (2010) 1202-1211.

[26] S. Sarina, H.Y. Zhu, Z.F. Zheng, S. Bottle, J. Chang, X.B. Ke, J.C. Zhao, Y.N. Huang, A. Sutrisno, M. Willans, G.R. Li, Chem. Sci. 3 (2012) 2138-2146.

[27] G. Palmisano, S. Yurdakal, V. Augugliaro, V. Loddo, L. Palmisano, Adv. Synth. Catal. 349 (2007) 964-970.

[28] S. Yurdakal, G. Palmisano, V. Loddo, V. Augugliaro, L. Palmisano, J. Am. Chem. Soc. 130 (2008) 1568-1569.

[29] L. Palmisano, V. Augugliaro, M. Bellardita, A. Di Paola, E.G. Lopez, V. Loddo, G. Marci, G. Palmisano, S. Yurdakal, Chemsuschem 4 (2011) 1431-1438.

[30] M. Zhang, C.C. Chen, W.H. Ma, J.C. Zhao, Angew. Chem. Int. Ed. 47 (2008) 9730-9733.

[31] Q. Wang, M. Zhang, C.C. Chen, W.H. Ma, J.C. Zhao, Angew. Chem. Int. Ed. 49 (2010) 7976-7979.

[32] X.J. Lang, H.W. Ji, C.C. Chen, W.H. Ma, J.C. Zhao, Angew. Chem. Int. Ed. 50 (2011) 3934-3937.

[33] Y.K. Zhang, W.T. Yang, Phys. Rev. Lett. 80 (1998) 890-890.

[34] S. Grimme, J. Antony, S. Ehrlich, H. Krieg, J. Chem. Phys. 132 (2010) 154104.

[35] Z.F. Zheng, H.W. Liu, J.P. Ye, J.C. Zhao, E.R. Waclawik, H.Y. Zhu, J Mol. Catal. A 316 (2010) 75-82.

[36] Z.F. Zheng, J. Zhao, Y. Yuan, H.W. Liu, D.J. Yang, S. Sarina, H.J. Zhang, E.R. Waclawika, H.Y. Zhu, Chem.-Eur. J. 19 (2013) 5731-5741.

[37] S. Furukawa, Y. Ohno, T. Shishido, K. Teramura, T. Tanaka, ACS Catal. 1 (2011) 1150-1153.

[38] S. Kim, W. Choi, J. Phys. Chem. B 109 (2005) 5143-5149.

[39] S. Furukawa, T. Shishido, K. Teramura, T. Tanaka, ACS Catal. 2 (2012) 175-179.

[40] X.J. Lang, W.H. Ma, Y.B. Zhao, C.C. Chen, H.W. Ji, J.C. Zhao, Chem.-Eur. J. 18 (2012) 2624-2631.

[41] H. Kobayashi, S. Higashimoto, Appl. Catal. B-Environ. 170–171 (2015) 135-143.

[42] D. Jiang, W.Z. Wang, E.P. Gao, L. Zhang, S.M. Sun, J. Phys. Chem. C 117 (2013) 24242-24249.

[43] S. Sarina, H.Y. Zhu, E.R. Jaatinen, Q. Xiao, H.W. Liu, J.F. Jia, C. Chen, J. Zhao, J. Am. Chem. Soc. 135 (2013) 5793-5801.

[44] L.M. Liu, B. McAllister, H.Q. Ye, P. Hu, J. Am. Chem. Soc. 128 (2006) 4017-4022.

[45] Z. Zhang, O. Bondarchuk, B.D. Kay, J.M. White, Z. Dohnalek, J. Phys. Chem. B 110 (2006) 21840-21845.

[46] I.M. Brookes, C.A. Muryn, G. Thornton, Phys. Rev. Lett. 87 (2001).

[47] M.B. Hugenschmidt, L. Gamble, C.T. Campbell, Surf. Sci. 302 (1994) 329-340.

[48] M.A. Henderson, Surf. Sci. 355 (1996) 151-166.

[49] M.A. Henderson, W.S. Epling, C.H.F. Peden, C.L. Perkins, J Phys. Chem. B 107 (2003) 534-545.

[50] R.M. Silverstein, F.X. Webster, D. Kiemle, Spectrometric identification of organic compounds, seventh ed., Wiley, New York, 2005.

[51] V. Augugliaro, V. Loddo, M.J. Lopez-Munoz, C. Marquez-Alvarez, G. Palmisano, L. Palmisano, S. Yurdakal, Photochemical & Photobiological Sciences 8 (2009) 663-669.

[52] V. Augugliaro, H. Kisch, V. Loddo, M.J. López-Muñoz, C. Márquez-Álvarez, G. Palmisano, L. Palmisano, F. Parrino, S. Yurdakal, Appl. Catal. A-Gen. 349 (2008) 189-197.

[53] J. Schneider, M. Matsuoka, M. Takeuchi, J. Zhang, Y. Horiuchi, M. Anpo, D.W. Bahnemann, Chem. Rev. 114 (2014) 9919-9986.

[54] C.L. Hawkins, D.I. Pattison, M.J. Davies, Amino Acids 25 (2003) 259-274.

[55] C.L. Hawkins, M.J. Davies, Free Radical Bio. Med. 39 (2005) 900-912.

[56] M. Zhang, Q. Wang, C.C. Chen, L. Zang, W.H. Ma, J.C. Zhao, Angew. Chem. Int. Ed. 48 (2009) 6081-6084.

Figure captions

Fig. 1. TEM micrograph of TiO_2(B) nanofibers covering with anatase nanoplates (BF). (A) Bright field image of TiO_2(B) nanofiber and anatase nanoplates with a size of about 30 nm. (B) Electron diffraction pattern of TiO_2(B) taken at [001] orientation. (C) HRTEM image showing anatase nanoplates on the surface of TiO_2(B). (D) The FFT image (the red square area in Panel a) which can be indexed as $[\bar{1}10]_{TB}$ //$[111]_{TA}$. (E) The IFFT image derived from FFT image showed the lattice fringes of two phases which are coincident well with anatase and TiO_2(B).

Fig. 2. Photocatalytic activity of TiO_2 (BF) and N-doped TiO_2 (N-BF) NFs in the selective aerobic oxidation reactions. Reaction conditions: 0.2 mmol reactant, 50 mg catalyst, 5 ml acetonitrile, 1 atm O_2, 40 °C, reaction time at 5 h and light intensity at 0.45 Wcm^{-2} (LED white light) for the oxidation of benzylamine, 4 h and 1 Wcm^{-2} (Xe light) for the oxidation of 4-methoxybenzyl alcohol.

Fig. 3. Influence of light intensity, wavelength and temperature on the phtotocatalytic aerobic oxidation of benzylamine. (A) The dependence of the catalytic activity of BF and N-BF NFs on the intensity of light irradiation. (B) Action spectrum for the aerobic oxidation of benzylamine on BF and N-BF NFs and differential UV-vis spectrum of bare catalyst and catalyst with adsorbed benzylamine. (C and D) Plot of benzylamine conversion rate *(C) versus* reaction time *t* at different temperatures under UV light (320-415 nm) and visible light (> 420 nm) irradiation.

Fig. 4. Influence of light intensity, wavelength and temperature on the phtotocatalytic aerobic oxidation of 4-methoxybenzyl alcohol. (A) The dependence of the catalytic activity of BF and N-BF NFs on the intensity of light irradiation. (B) Action spectrum for the aerobic oxidation of 4-methoxybenzyl alcohol on BF and N-BF NFs and differential UV-vis spectrum of bare catalyst

and catalyst with adsorbed 4-methoxybenzyl alcohol. (C and D) Plot of 4-methoxybenzyl alcohol conversion rate *(C) versus* reaction time *t* at different temperatures under UV light (320-415 nm) and visible light (> 420 nm) irradiation.

Fig. 5. The optimized structures of anatase TiO_2(100) surface (top view). (a-c) O_2 adsorption on TiO_2(100) surface with one -OH group; (d-f) O_2 adsorption on TiO_2(100) surface with -OH and -NH_2 groups; (g-h) O_2 adsorption on TiO_2(100) surface with two -OH groups and N replaced O on the surface. O, N, H and Ti atoms are marked in red, blue, green and grey.

Fig. 6. FT-IR spectra obtained after BF (A) and N-BF (C) NFs were exposed to 25 Pa benzylamine for various times. And FT-IR spectra of benzaldehyde adsorbed on (B) BF and (D) N-BF after evacuation and of benzylamine adsorbed on (B) BF and (D) N-BF after irradiation for various times under a dry air atmosphere. The green curves in the upper part of (B) and (D) stand for evacuation for 30 min after irradiation for 90 min.

Fig. 7. FT-IR spectra obtained after BF (A) and N-BF (C) NFs were exposed to 25 Pa 4-methoxybenzyl alcohol for various times. And FT-IR spectra of 4-methoxybenzaldehyde adsorbed on (B) BF and (D) N-BF after evacuation and of 4-methoxybenzyl alcohol adsorbed on (B) BF and (D) N-BF after irradiation for various times under a dry air atmosphere. The green curves in (B) and (D) stand for evacuation for 30 min after irradiation for 90 min. The green curves in the upper part of (B) and (D) stand for evacuation for 30 min after irradiation for 90 min.

Fig. 8. Schematic description of the proposed reaction mechanism for the photocatalytic aerobic oxidation of (A) benzylamine and (B) 4-methoxybenzyl alcohol.

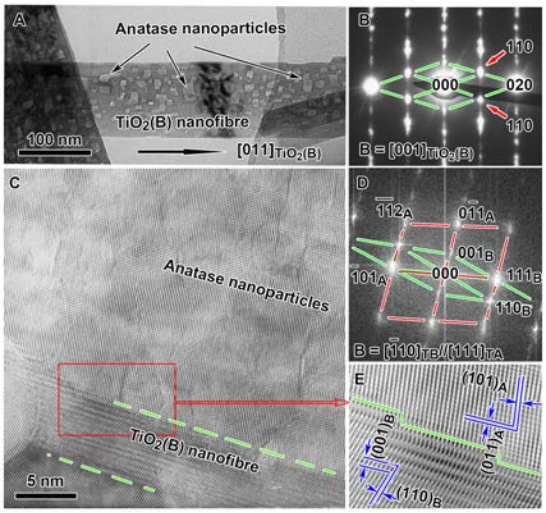
A
Anatase nanoparticles
TiO2(B) nanofibre
100 nm
[011]TiO2(B)
B
110
000
020
110
B = [001]TiO2(B)
C
Anatase nanoparticles
TiO2(B) nanofibre
5 nm
D
112A
011A
001B
101A
000
111B
110B
B = [1̄10]TB//[111]TA
E
(101)A
(001)B
(011)A
(110)B

Fig. 1.

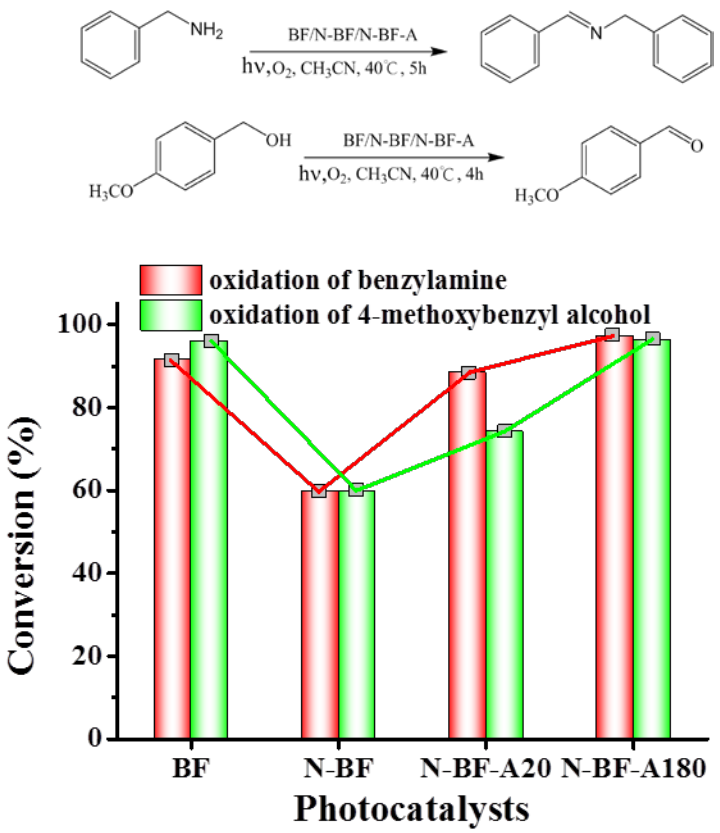
NH2
BF/N-BF/N-BF-A
hν,O2, CH3CN, 40℃, 5h
N
OH
H3CO
BF/N-BF/N-BF-A
hν,O2, CH3CN, 40℃, 4h
O
H3CO
oxidation of benzylamine
oxidation of 4-methoxybenzyl alcohol
Conversion (%)
100
80
60
40
20
0
BF
N-BF
N-BF-A20
N-BF-A180
Photocatalysts

Fig. 2.

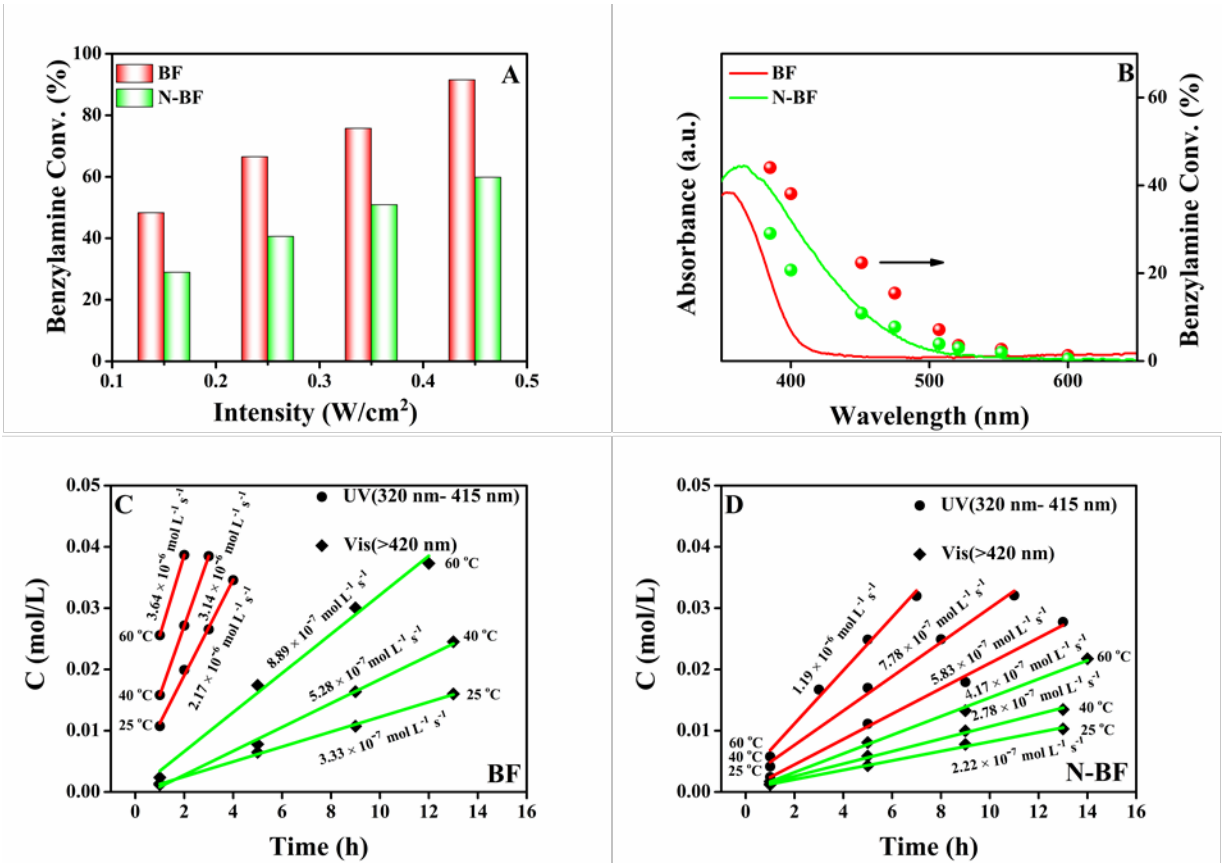
A
BF
N-BF
Benzylamine Conv. (%)
Intensity (W/cm²)
B
Absorbance (a.u.)
Benzylamine Conv. (%)
Wavelength (nm)
C
UV(320 nm- 415 nm)
Vis(>420 nm)
C (mol/L)
Time (h)
BF
D
N-BF

Fig. 3.

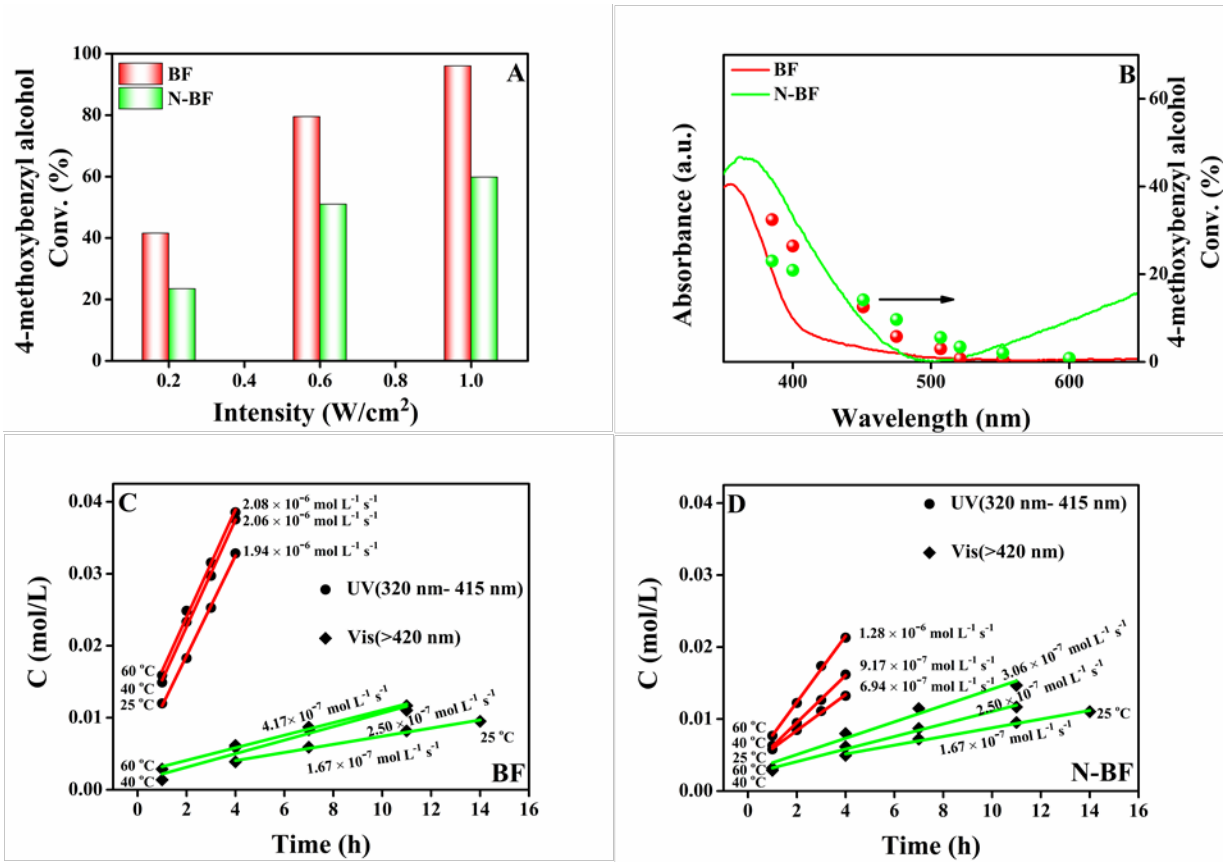
A
BF
N-BF
4-methoxybenzyl alcohol Conv. (%)
Intensity (W/cm^2)
B
Absorbance (a.u.)
Wavelength (nm)
C
UV(320 nm- 415 nm)
Vis(>420 nm)
C (mol/L)
Time (h)
D
N-BF

Fig. 4.

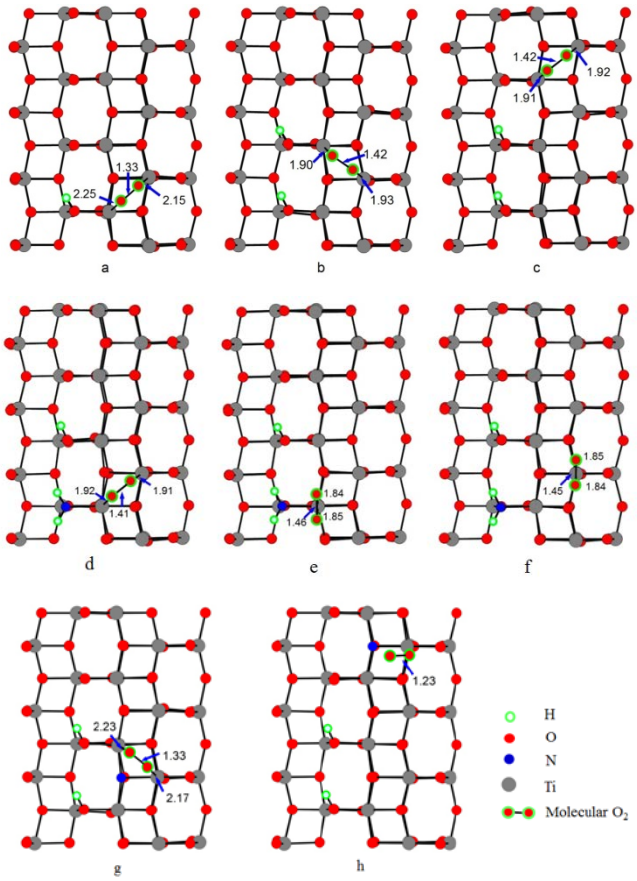
1.33
2.25
2.15
a
1.90
1.42
1.93
b
1.42
1.92
1.91
c
1.92
1.91
1.41
d
1.84
1.46
1.85
e
1.85
1.45
1.84
f
2.23
1.33
2.17
g
1.23
h
H
O
N
Ti
Molecular O2

Fig. 5.

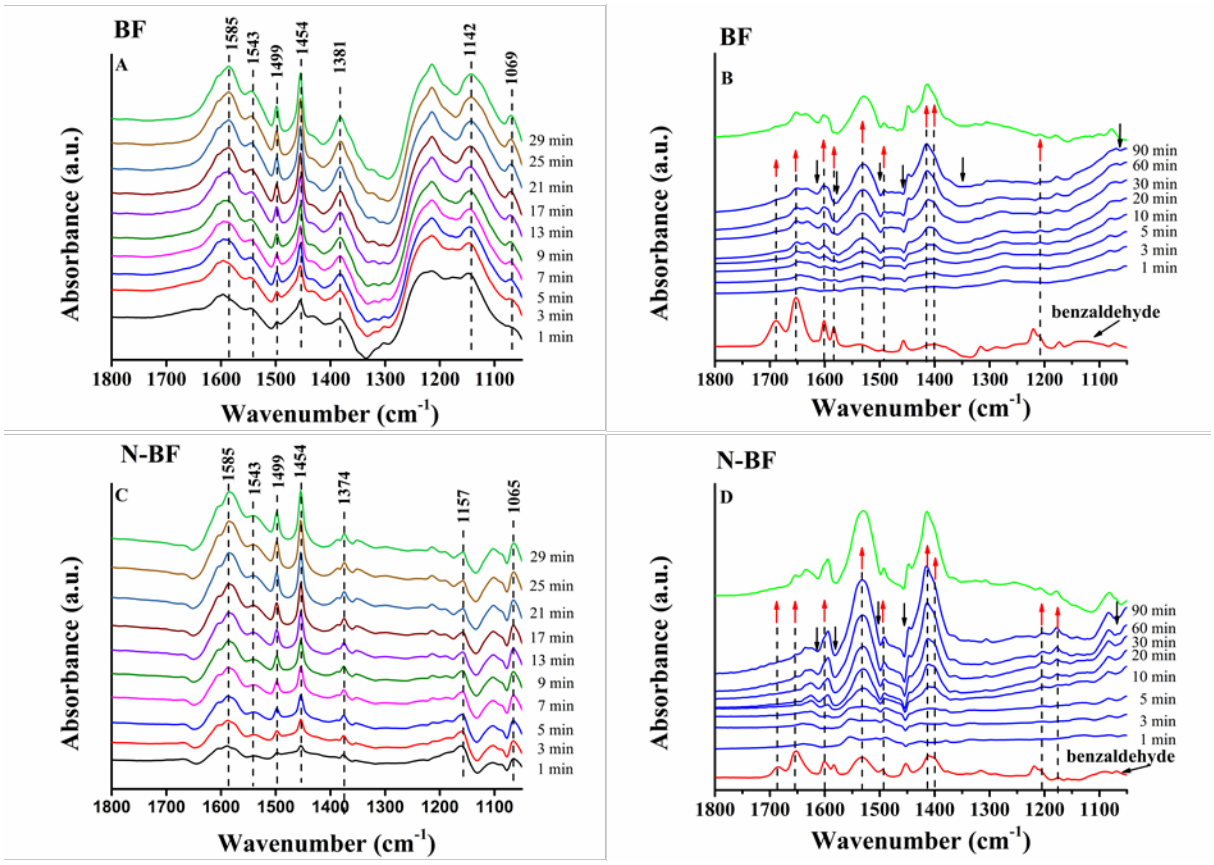
BF
A
1585
1543
1499
1454
1381
1142
1069
29 min
25 min
21 min
17 min
13 min
9 min
7 min
5 min
3 min
1 min
Absorbance (a.u.)
Wavenumber (cm-1)
BF
B
90 min
60 min
30 min
20 min
10 min
5 min
3 min
1 min
benzaldehyde
N-BF
C
1585
1543
1499
1454
1374
1157
1065
N-BF
D

Fig. 6.

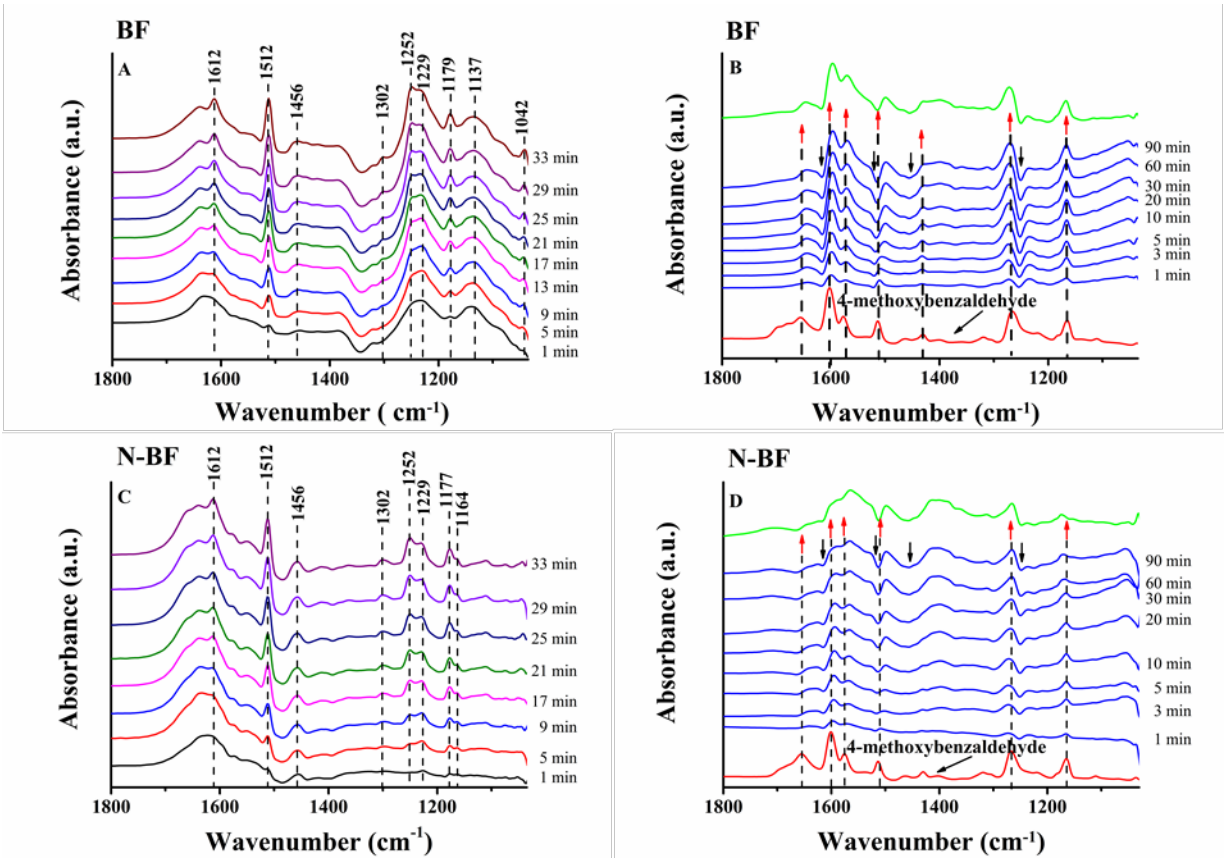
BF
A
1612
1512
1456
1302
1252
1229
1179
1137
1042
33 min
29 min
25 min
21 min
17 min
13 min
9 min
5 min
1 min
Absorbance (a.u.)
Wavenumber (cm⁻¹)
BF
B
90 min
60 min
30 min
20 min
10 min
5 min
3 min
1 min
4-methoxybenzaldehyde
Absorbance (a.u.)
Wavenumber (cm⁻¹)
N-BF
C
1612
1512
1456
1302
1252
1229
1177
1164
33 min
29 min
25 min
21 min
17 min
9 min
5 min
1 min
Absorbance (a.u.)
Wavenumber (cm⁻¹)
N-BF
D
90 min
60 min
30 min
20 min
10 min
5 min
3 min
1 min
4-methoxybenzaldehyde
Absorbance (a.u.)
Wavenumber (cm⁻¹)

Fig. 7.

A

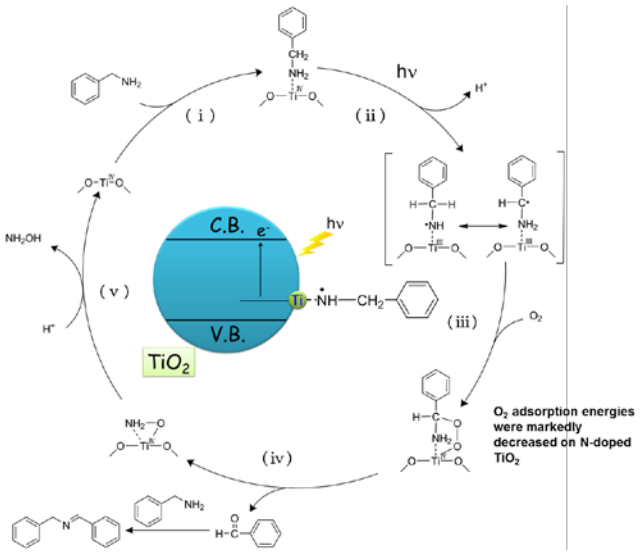
hν
(i)
(ii)
(iii)
(iv)
(v)
C.B.
V.B.
TiO2
O2 adsorption energies were markedly decreased on N-doped TiO2

B

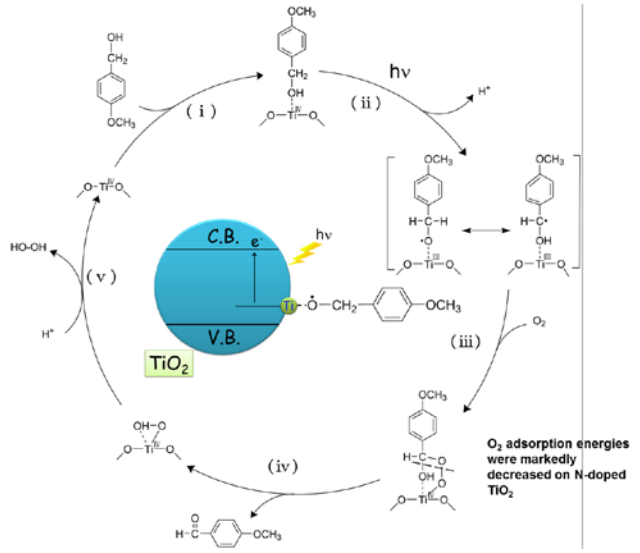
hν
(i)
(ii)
(iii)
(iv)
(v)
C.B.
V.B.
TiO2
O2 adsorption energies were markedly decreased on N-doped TiO2

Fig. 8.